Pertanika J. Trop. Agric. Sci. 49 (3): 1187 - 1216 (2026)

PERTANIKA JOURNALS

TROPICAL AGRICULTURAL SCIENCE

Journal homepage: http://www.pertanika.upm.edu.my/

The Effectiveness of Response Surface Methodology (RSM) as a Reliable Tool for Performance Optimisation in Azo Dye Removal Using Cellulose Nanofibril (CNF) Filter Paper

Siti Solehah Ahmad Norrahma[1], Nor Hazren Abdul Hamid[2]*, Nur Hanis Hayati Hairom[3], Latifah Jasmani[4], and Nurul Ain Mat Aron[1]

[1]Soil chemistry laboratory, Forestry Biotechnology Department, Forest Research Institute Malaysia (FRIM), 52109 Kepong, Selangor, Malaysia
[2]Faculty of Engineering Technology, Universiti Tun Hussein Onn Malaysia, Hab Pendidikan Tinggi Pagoh, KM 1, Jalan Panchor, 84600 Muar, Johor, Malaysia
[3]Microelectronic and Nanotechnology-Shamsuddin Research Centre (MiNT-SRC), Institute for Integrated Engineering, Universiti Tun Hussein Onn Malaysia, 86400 Parit Raja, Batu Pahat, Johor, Malaysia
[4]Pulp and Paper Branch, Forest Products Division, Forest Research Institute Malaysia, 52109 Kepong, Selangor, Malaysia

ABSTRACT

The potential of *Neolamarckia cadamba* cellulose nanofibril (CNF) filter paper as an azo dye treatment in a crossflow filtration system was investigated. The water permeability analysis was performed to assess the suitability of the fabricated CNF filter paper for filtration. Three operating parameters, cellulose dosage ratio, initial pH and initial concentration of methyl orange (MO) dye were optimised by central composite design (CCD) and response surface methodology (RSM). The results indicated that the model successfully predicted the relationship between the CNF filter paper and MO dye, demonstrating a high colour removal efficiency of 97.28% and an optimum normalised flux of 0.9748. These values were obtained under optimal conditions of a 50:50 cellulose ratio, pH 4, and an initial MO concentration of 600 mg/L. Fouling analysis using the Wiesner and Aptel model suggested that cake layer formation occurred in two stages under the optimum conditions. Overall, the findings indicate that RSM is useful for identifying suitable operating conditions, and the CNF filter paper shows good potential as a filtration material for azo dye removal.

Keywords: Cellulose nanofibril, crossflow filtration, membrane fouling mechanism, methyl orange, permeate flux, response surface methodology

ARTICLE INFO

Article history:
Received: 13 June 2025
Accepted: 03 June 2026
Published: 12 June 2026

DOI: https://doi.org/10.47836/pjtas.49.3.10

E-mail addresses:
solehahnorrahma91@gmail.com (Siti Solehah Ahmad Norrahma)
norhazren@uthm.edu.my (Nor Hazren Abdul Hamid)
nhanis@uthm.edu.my (Nur Hanis Hayati Hairom)
latifah@frim.gov.my (Latifah Jasmani)
NurulAinMatAron@gmail.com (Nurul Ain Mat Aron)
* Corresponding author

e-ISSN: 2231-8542

© Universiti Putra Malaysia Press

INTRODUCTION

With the various environmental concerns, the growing amount of contaminated wastewater released into aquatic systems in textile and related industries, with the use of synthetic dyes, has become a major concern. Industries such as textiles, paper, leather, and cosmetics contribute significantly to dye pollution because of the extensive use of colouring agents during manufacturing processes (Javaid et al., 2021). Most synthetic dyes are difficult to degrade owing to their stable chemical structures and resistance to biological decomposition. Their resistance to degradation allows the dyes to remain in the environment for long periods. Previous studies have reported that exposure to certain synthetic dyes may cause adverse effects on human health, including skin and eye irritation, liver damage, and potential mutagenic or carcinogenic effects (Singh et al., 2021; Thiruppathi et al., 2021).

Various methods have been explored for the removal of dyes from wastewater, such as adsorption (Hanafy, 2021; Hussain et al., 2021; Lin et al., 2021a), oxidation processes (Pu et al., 2022; Türgay et al., 2011), electrochemical treatment (Petcu et al., 2016), and nanofiltration membrane systems (Amin & Nizam, 2016; Aryanti et al., 2018; Bai et al., 2023; Miao et al., 2021). Cellulose nanofibril (CNF) nanopapers have been the focus of study in recent years for use as a membrane because of the excellent adsorption properties and the possibility of using them for filters in wastewater treatment. Although these benefits, their usage is still restricted due to the low water permeability based on the dense fibre structure. Hence, efforts towards the development of nanopaper need to be directed towards the creation of a porous network of cellulose with an appropriate pore size to enhance the water transport performance (Mautner et al., 2019). Porosity-enhancing cellulose-based membranes were reported to render good mechanical stability along with a high rejection performance by Gu et al. (2023).

CNF has been manufactured from various sources of raw materials, such as wood-based materials, non-wood fibres and agricultural wastes. *Neolamarckia cadamba* or locally known as *Kelempayan,* is one of the possible materials, commonly available in South China and South Asian countries. The tropical wood species is a high cellulose content wood species, which is suitable to be used for the production of bleached pulp and then used for the production of CNF (Latifah et al., 2020). The tree species used in this study was *Neolamarckia cadamba* due to its availability from forest plantations in Malaysia and its potential for developing value-added CNF filter paper material.

In this study, nanofiltration membrane technology incorporated into a crossflow filtration system was investigated as an alternative approach due to its capability to provide more consistent and sustainable filtration performance. Cross-flow filtration systems are typically continuous filtering systems adapted from hybrid membrane photocatalytic reactors (MPR). The permeation of the treated solution influences the efficiency and capabilities of this system (Desa et al., 2019; Hairom et al., 2015; Sidik et al., 2019).

Compared with traditional filtration methods, the crossflow filtration system employs continuous tangential flow to reduce pollutant transport into the treated effluent.

Design of Experiments (DOE) is a group of strategies and processes used primarily to investigate data referring to specific variables of a particular subject of study (El-Sheekh et al., 2023). To maximise the filtration of textile wastewater utilising CNF filter paper, the experimental factorial design of the central composite design (CCD) was implemented in this study. Meanwhile, response surface methodology (RSM) is an empirical approach based on the DOE principle, which is used in the design, modelling, and optimisation of experimental factors and their interactions with responses, compared to the one-factor-at-a-time technique (K et al., 2021; Yadav et al., 2021; Veza et al., 2023). The application of RSM has evolved from simple optimisation to complex fouling analysis, as demonstrated by Chen et al. (2024), who utilised RSM to decode the interactions between operational variables and membrane life-cycles. This study is an extension of these developments using a fine-tuned CCD-RSM for processing *Neolamarckia cadamba*, the unique feedstock.

Membrane fouling behaviour was analysed using the Wiesner and Aptel model, which was adapted from Hermia's classical blocking filtration laws (Hermia, 1985; Wiesner & Aptel, 1996). The modelling approach assumed constant membrane resistance, consistent pressure drops, and stable specific cake resistance throughout the filtration process (Desa et al., 2019). In addition, the experimental data enabled further interpretation of the flux decline behaviour during the filtration process.

Although cellulose-based nanopapers have been widely investigated for dye adsorption and dead-end filtration applications, studies focusing on the optimisation of methyl orange (MO) removal using enzymatically pre-treated *Neolamarckia cadamba* CNF filter paper in a continuous crossflow filtration system remain limited. This study addresses this gap by establishing a predictive model for both colour removal and flux decline mechanisms in a crossflow configuration. Thus, the CCD model designed based on RSM was implemented to assess the performance of the CNF filter paper and the optimum conditions based on the parameters. Blocking mechanism analysis was further employed to investigate the flux decline behaviour and to explain the fouling progression occurring on the nanocellulose filter paper surface.

MATERIALS AND METHODS

Reagents and Materials

In this study, only analytical-grade chemicals and reagents were employed. Sulphuric acid (96%) was purchased from Fisher Scientific (UK), and fully hydrolysed polyvinyl alcohol (PVA) was obtained from Sigma Aldrich (US). Sodium hydroxide, sodium sulphide, ethanol, and toluene were purchased from R&M Chemical (UK), while glacial acetic acid was acquired from Ajax Finechem (Australia) and sodium chlorite from Merck (USA). R&M Chemicals (UK) supplied the methyl orange (MO) powder.

MO Dye Solution Preparation

Distilled water was used to dissolve the pigment powder at concentrations of 100-1000 mg/L to produce dye solutions. The colour intensity of the MO dye was measured by utilising a Hitachi U-3900H UV-Vis Spectrophotometer. Hydrochloric acid (HCl) and sodium hydroxide (NaOH), both manufactured by R&M Chemicals (UK), were utilised for modifying the pH. The pH was determined using a microprocessor pH metre (HQ440d multi, Hach Model). No additional buffer solutions or reagents were used during the UV-Vis absorbance measurement, apart from the HCl and NaOH used for the pH adjustment of the dye solution before analysis.

Enzymatically Pre-treated *Neolamarckia cadamba* Cellulose Nanofibril Filter Paper

In accordance with previously published work by Latifah et al. (2020), cellulose nanofibrils (CNF) from *Neolamarckia cadamba* were synthesised through kraft pulping and bleaching processes. Cellulase enzyme from *Aspergillus niger* was used as an enzymatic pre-treatment to continue the process. Approximately 2300 g of bleached pulp from the previous process stage was mixed with 8.2 g of sodium acetate ($C_2H_3NaO_2$), 2.5 g of cellulase enzyme, and 2.0 L of distilled water. The enzymatic reaction procedure was carried out for 72 hours under operational conditions with a stirring rate of 80 rpm and a temperature of 28 °C. The sample was then soaked in hot water to denature the enzyme reaction.

The preparation and fabrication procedures employed in this study were adapted from the method reported by Norrahma et al. (2023). The CNF filter paper used in this study was prepared by combining cellulose nanofibrils (CNF) and bleached pulp at various mixing ratios, namely 50:50, 60:40, 70:30, 80:20, and 90:10.

Physical Characterisation of CNF Filter Paper

Physical characterisation of the CNF filter paper was carried out by evaluating its thickness, density, porosity, and fibril diameter (Mautner & Bismarck, 2021). Thickness measurements for each cellulose composition were obtained using an L&W Micrometre instrument (Lorentzen and Wettre) at ten different locations, followed by calculation of the average value. The fibril diameters were subsequently determined through 30 repeated measurements using the Fiji distribution plugin in ImageJ (Java 8).

The mass (m, g) and thickness (d, μm) of the CNF filter paper were measured to evaluate the grammage (G, g/m²), envelope density (ρe), and porosity (Φ) based on established methods reported by Janesch et al. (2020). Mass measurements were obtained using an analytical balance (A&D GF-1600, US), whereas thickness was determined using an L&W Micrometre (Code 250, Lorentzen and Wettre). The theoretical porosity was subsequently calculated using the theoretical density of pure cellulose (ρc = 1500 kg/m³)

as reported by Mautner and Bismarck (2021). Equations 1, 2, and 3 were applied to determine the grammage, envelope density, and porosity values, respectively.

$$G(gm^{-2}) = \frac{m\ (g)}{\pi r^2\ (m^2)} \quad [1]$$

$$\rho_{envelope}\ \ (kgm^{-3}) = \frac{G\ (kgm^{-2})}{d\ (m)} \quad [2]$$

$$\Phi\ (\%) = (1 - \frac{\rho_{envelope}\ \ (kgm^{-3})}{\rho_{cellulose}\ \ (kgm^{-3})}\ x\ 100) \quad [3]$$

Water Permeability Testing

The water permeability test was carried out by exposing the CNF filter paper to continuous distilled water circulation at 3 bars pressure for 30 minutes during the wetting process to avoid recurring membrane compaction. A schematic representation of the crossflow filtration setup is shown in Figure 1, comprising a 2 L reactor tank coupled with a separation unit. The permeation study was conducted using a Sterlitech™ HP4750 (USA) crossflow filtration system with CNF filter paper providing an effective filtration area of 20.60 cm².

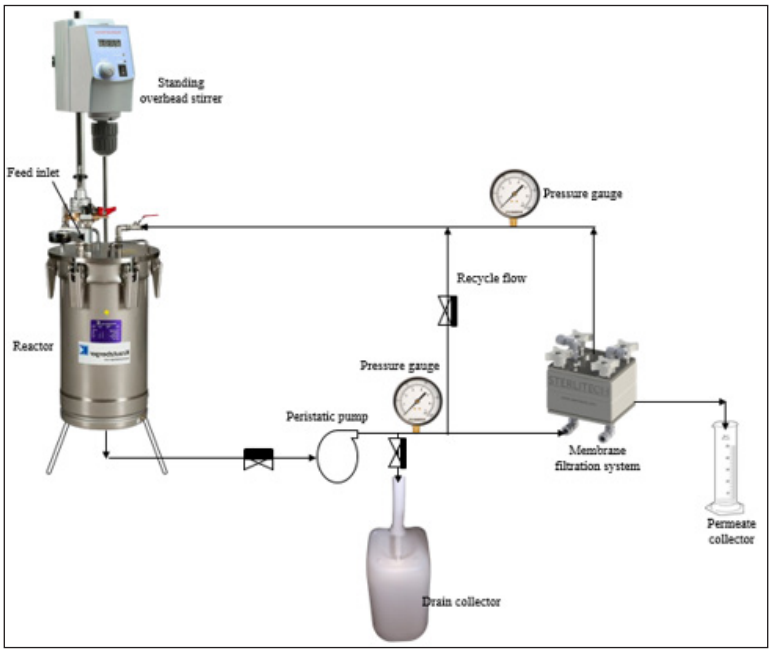

Figure 1. Schematic diagram of a crossflow filtration system

Experimental Set-up

Following the procedure established in the previously published work by Norrahma et al. (2023), various CNF filter papers with mixing ratios of CNF and bleached pulp at 50:50, 60:40, 70:30, 80:20, and 90:10 were integrated into the filtration system. The cellulose dosage was fixed at 50:50 for the RSM optimisation phase based on its superior permeability performance (229.04 $Lm^{-2}hr^{-1}$) (Norrahma et al., 2023). During the scoping experiments, the initial pH of the MO dye solution was adjusted within the range of 3.0-10.0, whereas the dye concentration varied from 100 to 600 mg/L. Permeate flux readings were monitored every 5 minutes throughout the 3-hour filtration process. The CNF filter paper performance was then assessed under the optimal operating conditions identified in this study, namely the cellulose composition ratio, solution pH, and initial dye concentration.

Preliminary Scoping and Parameter Selection

Initial scoping experiments were first performed to establish the appropriate operating range for each experimental variable before implementing the CCD model (Hamid et al., 2016). In this study, pH (X_1) and initial MO dye concentration (X_2) were treated as independent variables, whereas colour removal (Y_1) and normalised flux (Y_2) represented the dependent responses. The range of each parameter was selected according to the findings obtained from the preliminary screening experiments.

The pH range investigated in this study was selected between 3 and 10 to represent acidic and alkaline wastewater conditions commonly applied in dye treatment studies (Amin & Nizam, 2016; Hairom et al., 2014). The dye concentration range used in this study was selected according to the ability of the CNF filter paper to remove contaminants at different concentration levels, as reported in previous studies (Hussain et al., 2021; Lin et al., 2021). Several operating conditions were fixed throughout the experiment, including the cellulose dosage ratio (50:50), operating pressure (3 bars), and filtration time (3 hours), based on the preliminary scoping tests. The applied pressure was suitable to prevent damage or rupture of the filter paper during filtration. At the same time, the filtration time selected was thought to be adequate for the system to be settled. Consequently, MO dye removal through the crossflow filtration system was evaluated at pH 3-10 and dye concentrations ranging from 100 to 600 mg/L.

Statistical Optimisation via CCD-RSM

Central composite design (CCD) in the response surface methodology (RSM) was selected in this study due to its capability to efficiently develop second-order polynomial models with a reduced number of experimental runs. Compared to conventional one-factor-at-a-time approaches, CCD allows the evaluation of interaction and quadratic effects between operational variables, making it suitable for optimisation studies involving nonlinear filtration systems.

In addition, CCD provides a reliable prediction of system performance while minimising experimental cost and time. CCD-RSM analysis was performed using Design-Expert software (Stat-Ease Inc., version 13) for experimental design, statistical modelling, response surface generation, and optimisation analysis. The relationship between the independent variables, namely pH (X_1) and initial feed concentration (X_2), and the response variables, colour removal (Y_1) and normalised flux (Y_2), was subsequently evaluated. Preliminary experiments for scoping were performed to establish the selected parameters and ranges. The optimisation study was done using pH range of 4 - 9 and initial MO dye concentration of 300 - 600 mg/L. The CCD matrix was developed from the coded level low (−1) and high (+1) of the operating conditions.

Analytical Methods

Colour concentration measurements were performed using a UV-Vis spectrophotometer (Hitachi, U-3900H) at the maximum absorption wavelength of λmax = 465 nm. The degradation of the dye solution was determined from the decrease in absorbance intensity recorded at the maximum wavelength. The percentage of colour removal was then calculated using the following Equation 4.

$$\frac{C_0 - C_t}{C_0} \times 100\% \quad [4]$$

where C_0 denotes the initial colour concentration of the dye solution, whereas C_t corresponds to the remaining colour concentration after filtration at a given reaction time.

The pure water flux (J_0) of each CNF filter paper was calculated based on the permeate volume (V) passing through a unit membrane area (A) within a given filtration time (t), using the following Equation 5:

$$J_0 = \frac{V}{At} \quad [5]$$

In the periods of time t_1 and t_2, the instantaneous permeate flow (J) at each run was determined by Equation 6:

$$J = \frac{V_2 - V_1}{A(t_2 - t_1)} \quad [6]$$

Equation 7 was applied to normalise the flux values to assess the filtration performance of the CNF filter paper under varying operational parameters. The reduction in permeate flow was further evaluated by presenting the normalised flux profile against operating time.

$$Normalised\ flux = \frac{Solution\ \ flux\ J}{Pure\ \ water\ \ flux\ J_0} \quad [7]$$

Membrane Fouling Mechanism

The fouling mechanism of the CNF filter paper at the optimum filtration condition was analysed based on the Wiesner and Aptel models. MATLAB R2023b was used to generate the blocking law plots and determine the corresponding fitting parameters from the filtration time data. The dominant fouling mechanism was identified using the fitted rate constant (K) and coefficient of determination (R^2) values. The general equation used to analyse blocking filtration laws is presented in Equation 8, where V is the volume of permeate at time, t, and K is the coefficient depending on the flow rate and solution properties.

$$\frac{d^2t}{dV^2} = K \times \left(\frac{dt}{dV}\right)n \quad [8]$$

RESULTS AND DISCUSSION

Physical Properties and Performance of CNF Filter Paper

Figure 2 presents the envelope density and porosity behaviour of CNF filter paper as a function of thickness for different cellulose dosage compositions. Increasing the CNF proportion in the CNF-bleached pulp matrix resulted in a noticeable reduction in filter paper thickness, decreasing from 306.8 ± 5.2 µm at the 50:50 composition to 83.9 ± 4.5 µm at the 90:10 composition. At the same time, the envelope density increased from 195.61 to 716.51 kg/m³ as the CNF concentration increased. Based on the theoretical density of pure cellulose (1500 kg/m³), the porosity (Φ) ranged from 13.04% to 47.68% when the filter paper thickness decreased. This observation indicates that higher CNF content led to closer fibre arrangement, producing a denser and more compact filter paper structure.

A decrease in water permeance was observed as the cellulose dosage of the CNF filter paper increased. This may be related to the formation of a denser fibre network with fewer empty spaces, making it more difficult for water molecules to pass through the filter paper. Similar behaviour was observed from the porosity results of the fabricated CNF filter paper.

The thickness and fibril diameter of the CNF filter paper prepared with different dosage ratios of cellulose are shown in Figure 3. The thickness of the filter paper slowly decreased as the CNF content increased, while the fibril diameter increased proportionately with the CNF content. According to Mautner and Bismarck (2021), fibril network porosity is among the key factors affecting the fibril diameter within nanocellulose paper structures. The physical properties obtained for all CNF filter paper compositions are summarised in Table 1. The observed increase in porosity may be attributed to the formation of compact and densely packed nanofibrillated cellulose networks during the pressing process, which subsequently influenced the development of the fibril structure.

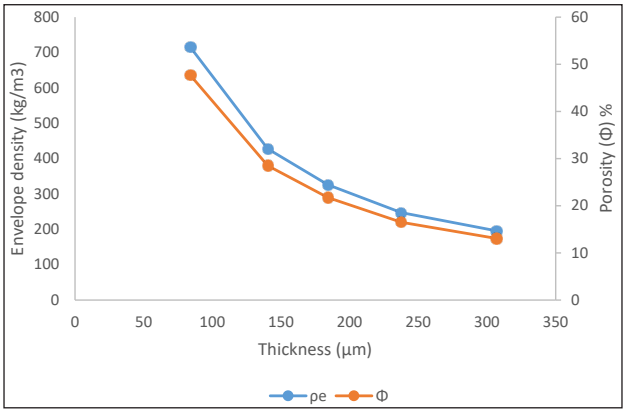

Figure 2. Envelope density and porosity evaluation based on the thickness value of the CNF filter paper

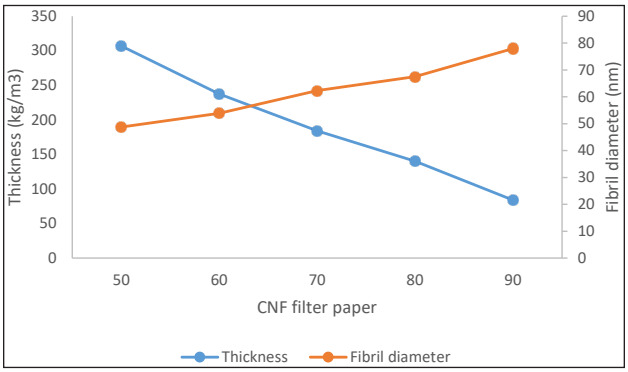

Figure 3. Effect of cellulose dosage on the thickness and fibril diameter of CNF filter paper

Table 1
Composition of G (grammage), thickness (d), envelope density (ρ_e), porosity (Φ), and fibril diameters of CNF filter paper

Mixing Ratio		G (g/m^2)	d± Std. dev. (µm)	ρ_e ±Std. dev. (kg/m^3)	Φ (%)	Fibril Diameter (nm)		
CNF	Bleached Pulp					Average	Max.	Min.
50	50	60	306.8 ± 5.2	195.61 ± 2.7	13.04	48.8 ± 18.8	105.404	19.348
60	40	60	237.6 ± 4.4	247.07 ± 3.7	16.47	53.8 ± 26.4	127.03	17.959
70	30	60	184.1 ± 11.4	326.75 ± 16.5	21.73	62.3 ± 22.3	95.817	4.277
80	20	60	140.3 ± 5.6	428.11 ± 13.9	28.51	67.5 ± 18.9	89.119	15.375
90	10	60	83.9 ± 4.5	716.51 ± 1.4	47.68	77.9 ± 51.8	171.055	16.141

Note. Std. dev. = standard deviation

Water Permeability Assessment

Maintaining stable water permeability with minimal permeance variation after membrane compaction is considered an important characteristic of high-performance membranes (Mautner & Bismarck, 2021). Despite their high rejection capability, many nanocellulose membranes remain limited by low permeability performance (Yousefi et al., 2021). Accordingly, this study evaluated the compatibility of the fabricated CNF filter paper within the crossflow filtration system under pollutant-free conditions using distilled water. The profile of distilled water flux for each CNF filter paper composition is shown in Figure 4 at different pressures of operation. Linear regression coefficient (R^2) was used to assess the consistency of membrane performance. The values of R^2 for all cellulose dosage compositions were above 0.90, which indicates good membrane performance. At 3 bars operating pressure, the permeability values for the 50:50, 60:40, 70:30, and 80:20 compositions were 229.0396, 63.7684, 8.5732, and 231.6199 $Lm^{-2}h^{-1}$, respectively. The 90:10 composition, on the other hand, ruptured the membrane at 1 bar and was not used for further analysis.

Maintaining high density alongside high porosity while yielding high permeance is a primary objective for high-quality nanopapers. This study demonstrates that the CNF filter paper is compatible with the crossflow filtration system at cellulose dosages of 50:50, 60:40, 70:30, and 80:20. The observed compatibility can be related to the formation of looser fibril networks that promoted higher porosity and greater void volume within the CNF filter paper. Despite the increased resistance caused by denser fibre packing, the addition of bleached pulp during fabrication enabled the development of larger pore structures while maintaining nanopaper density. Consequently, this contributed to the permeance behaviour and compatibility performance observed in the crossflow filtration system.

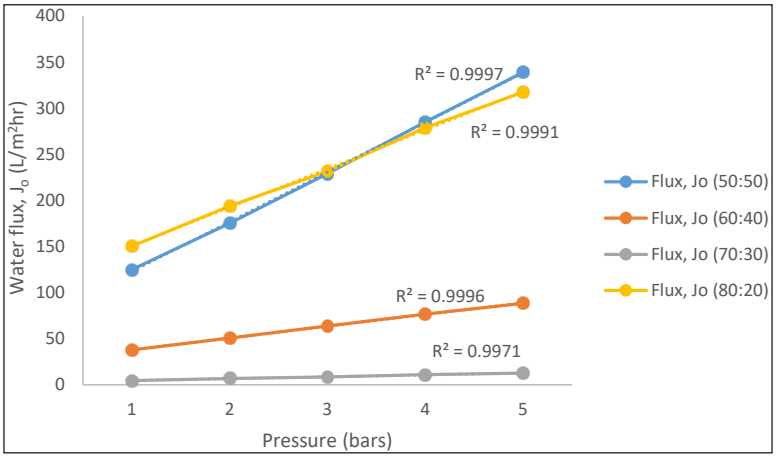

Figure 4. Distilled water flux against pressure for various cellulose dosages of CNF filter paper

CCD-RSM Optimisation for MO Dye Removal using CNF Filter Paper

CCD-RSM was employed to establish the relationship between the selected operating variables and the filtration responses. The experimental design generated 13 runs based on a 2^2 full factorial central composite design consisting of two independent variables: pH (X_1) and initial MO dye concentration (X_2). Colour removal (Y_1) and normalised flux (Y_2) were selected as the response variables for model evaluation. The CCD arrangement included four factorial points, four axial points, and five replicated centre points to estimate experimental uncertainty and to verify the reproducibility and suitability of the proposed model. Table 2 shows the coded factors and range and levels of independent variables, while the experimental design and corresponding results are presented in Table 3. The experimental findings demonstrated that the highest colour removal (97.28%) and normalised flux (0.9748) were achieved at the factorial design point corresponding to pH 4 and 600 mg/L initial MO dye concentration. Conversely, the centre point condition (pH 6.5 and 450 mg/L) produced the lowest performance, with colour removal and normalised flux values of 70.80% and 0.1836, respectively. The predicted responses for colour removal percentage and normalised flux were described by the second-order polynomial equation in Equation 9.

$$Y = \beta_0 + \Sigma_{i=1}^{k}\beta_i X_i + \Sigma_{i=1}^{k}\beta_{ii} X_i^2 + \Sigma_{i<j}\beta_{ij} X_i X_j + \varepsilon \quad [9]$$

where Y is the measured response; x_i and x_j are the coded independent variables; β_0, β_i, β_{ii}, and β_{ij} are the regression constant, linear, quadratic, and interaction coefficients, respectively; and ε is the random error.

Table 2
Experimental ranges and levels of independent variables

Independent Variable	Factor Code	Range and Level				
		-α	**-1**	**0**	**+1**	**+α**
Initial pH	X_1	4	2.96	6.5	10.04	9
Initial MO dye concentration (mg/L)	X_2	300	237.87	450	662.13	600

Table 3
Experimental conditions and results of responses from the CCD

Run	Experimental Variable		Response (Colour Removal, Y_1)		Responses (Normalised Flux, Y_2)	
	pH, X_1	Concentration, X_2 (mg/L)	Experimental	Predicted	Experimental	Predicted
1	4	600	97.28	97.08	0.9748	0.9671
2	6.5	450	50.25	51.07	0.5247	0.5601
3	9	300	62.17	61.97	0.1954	0.1877
4	6.5	450	52.60	51.07	0.5695	0.5601
5	4	300	93.10	92.90	0.8745	0.8668
6	9	600	87.04	86.84	0.1589	0.1512
7	6.5	450	50.30	51.07	0.5742	0.5601
8	10	450	75.99	76.19	0.2957	0.3034
9	6.5	450	51.4	51.07	0.5484	0.5601
10	3	450	90.75	90.95	0.7251	0.7328
11	6.5	240	91.52	91.72	0.3756	0.3833
12	6.5	450	50.80	51.07	0.5836	0.5601
13	6.5	660	79.71	79.91	0.7458	0.7535

Model Fitting and Analysis of Variance

ANOVA was applied to assess the suitability of the quadratic polynomial model and to analyse the effects of the independent variables and their interactions on the response parameters (Esmi et al., 2023). The suitability of the second-order regression model was assessed using several statistical criteria, including the sequential Fisher test (F-test), lack-of-fit analysis, and other CCD adequacy parameters (Kadier et al., 2022). The statistical outcomes for each response are presented in Table 4. In general, a significant quadratic model is associated with high F-values and low probability values. The developed models in this study produced F-values of 18.05 for colour removal and 6.62 for normalised flux. Model significance was further interpreted based on the 'Prob > F' values, where values lower than 0.05 indicate statistical significance, whereas values greater than 0.1 represent insignificant model parameters. The initial ANOVA results suggested that both response models (Y1 and Y2) were statistically insignificant.

A developed model is typically considered reliable when the lack-of-fit result is statistically insignificant ($P > 0.05$), suggesting good agreement between the predicted and experimental data (Esmi et al., 2023). In ANOVA analysis, the lack-of-fit test is used to determine the suitability of the regression model within the investigated experimental range. Significant lack of fit may indicate that the model is unable to adequately represent the experimental behaviour due to unaccounted variations or insufficient regression fitting (Favier et al., 2023; Kadier et al., 2022). As shown in Table 4, the initial models for Y1 and Y2 exhibited significant lack-of-fit behaviour, with F-values of 110.34 and 75.00 and associated probability values of 0.0003 and 0.0004, respectively. This initial analysis indicated that the full quadratic model was insufficient ($P < 0.05$ for lack of fit). To improve accuracy, a stepwise algorithm was employed to select significant cubic terms and eliminate insignificant interactions. This resulted in a refined model that demonstrated high significance ($P < 0.0001$) and a non-significant lack of fit, making it suitable for optimisation (Favier et al., 2023). The final empirical quadratic equations describing the response functions are presented in Equations 10 and 11.

$$\text{Colour removal (\%) } (Y_1) = 51.07 - 5.22X_1 - 4.18X_2 + 5.17X_1X_2 + 16.25X_1^2 + 17.37X_2^2 + 11.44\,X_1^2X_2 - 5.07\,X_1X_2^2 \quad [10]$$

$$\text{Normalised flux } (Y_2) = 0.5601 - 0.1518X_1 + 0.1309X_2 - 0.0342X_1X_2 - 0.0210X_1^2 + 0.0041X_2^2 - 0.1149\,X_1^2X_2 - 0.2219\,X_1X_2^2 \quad [11]$$

The final reduced cubic models for Y_1 and Y_2 incorporated two linear terms (X_1 and X_2), a second-order interaction term (X_1X_2), two quadratic terms (X_1^2 and X_2^2), and two cubic interaction terms ($X_1^2X_2$ and $X_1X_2^2$). The statistically significant parameters identified after stepwise regression analysis are presented in Table 4, where all retained terms satisfied the significance requirement of $p < 0.05$. For colour removal (Y_1), all model terms were statistically significant, with X_2^2 representing the dominant contributor to the ANOVA model. Meanwhile, the significant contributors for normalised flux (Y_2) were limited to X_1, X_2, $X_1^2X_2$, and $X_1X_2^2$. Model reduction was performed to eliminate insignificant terms and improve the adequacy of the regression models. The results of the analysis of variance for the modified response variables are presented in Table 5. The F-values of the adjusted models were substantially higher and accompanied by lower P-values, indicating improved model significance and predictive capability. High F-values of 764.31 and 192.69 for Y_1 and Y_2, respectively, together with probability values below 0.0001, confirmed the adequacy and statistical significance of the developed models (Ecer et al., 2024). The resulting lack-of-fit and probability values further supported the predictive reliability of the regression models.

Table 4
ANOVA results for the investigated response variables

Source	Colour Removal (%) Response						Contribution (%)
	Sum of Square	df	Mean Square	F-value	P-value (Prob>F)	Remarks	
Model	4091.19	5	818.24	18.05	0.0007	Not significant	
X_1	481.18	1	481.18	10.62	0.0139		10.59
X_2	19.06	1	19.06	0.4205	0.5374		0.42
X_1X_2	107.02	1	107.02	2.36	0.1683		2.35
X_1^2	1837.24	1	1837.24	40.54	0.0004		40.43
X_2^2	1837.24	1	1837.24	46.33	0.0003		46.21
Lack of fit	313.47	3	104.49	110.34	0.0003	Significant	
Source	**Normalised Flux Response**						**Contribution (%)**
	Sum of Square	**df**	**Mean Square**	**F-value**	**P-value (Prob>F)**	**Remarks**	
Model	0.6036	5	0.1207	6.62	0.0139	Not significant	
X_1	0.5524	1	0.5524	30.30	0.0009		91.54
X_2	0.0431	1	0.0431	2.37	0.1680		7.16
X_1X_2	0.0047	1	0.0047	0.2566	0.6280		0.78
X_1^2	0.0031	1	0.0031	0.1683	0.6939		0.51
X_2^2	0.0001	1	0.0001	0.0066	0.9377		0.02
Lack of fit	0.1254	3	0.0418	75.00	0.0004	Significant	

Table 5
ANOVA results for the modified response variable

Source	Colour Removal (%) Response						Contribution (%)
	Sum of Square	df	Mean Square	F-value	P-value (Prob>F)	Remarks	
Model	4404.34	7	629.19	764.31	<0.0001	Significant	
X_1	108.93	1	108.93	132.32	<0.0001		2.40
X_2	69.74	1	69.74	84.71	0.0003		1.54
X_1X_2	107.02	1	107.02	130.00	<0.0001		2.36
X_1^2	1837.24	1	1837.24	2231.80	<0.0001		40.50
X_2^2	2099.81	1	2099.81	2550.75	<0.0001		46.29
$X_1^2X_2$	261.65	1	261.55	317.85	<0.0001		5.77
$X_1X_2^2$	51.49	1	51.49	62.55	0.0005		1.14
Lack of fit	0.3280	1	0.3280	0.3464	0.5878	Not significant	
Source	**Normalised Flux Response**						**Contribution (%)**
	Sum of Square	**df**	**Mean Square**	**F-value**	**P-value (Prob>F)**	**Remarks**	
Model	0.7286	7	0.1041	192.69	<0.0001	Significant	
X_1	0.0922	1	0.0922	170.68	<0.0001		31.41
X_2	0.0685	1	0.0685	126.86	<0.0001		23.25
X_1X_2	0.0047	1	0.0047	8.66	0.0321		1.59
X_1^2	0.0031	1	0.0031	5.68	0.0629		1.05
X_2^2	0.0001	1	0.0001	0.2215	0.6577		0.04
$X_1^2X_2$	0.0264	1	0.0264	48.91	0.0009		9.00
$X_1X_2^2$	0.0985	1	0.0985	182.38	<0.0001		33.56
Lack of fit	0.0005	1	0.0005	0.8455	0.4099	Not significant	

Model Adequacy

Table 6 presents the coefficient of determination (R^2) values used to assess the adequacy of the developed regression models. The R^2 parameter reflects the degree of agreement between the predicted and experimental data by representing the ratio of explained variation to total variation (Zhou et al., 2023). A model is generally considered to exhibit better fitting performance when the R^2 value approaches 1 (Favier et al., 2023). In this study, high R^2 values of 0.9991 for colour removal and 0.9963 for normalised flux confirmed excellent agreement between the predicted and observed responses. The good agreement between the experimental and predicted data was obtained for the developed models, as shown in Figures 5(a) and 6(a). This behaviour could be attributed to the entrapment of MO dye molecules in the void spaces of the fibril network, which resulted in a lower permeate transport rate but higher dye retention. Also, the difference in adjusted R^2 and predicted R^2 for both responses was less than 0.2, which was acceptable for the developed models

to describe the filtration performance. The colour removal model produced adjusted and predicted R^2 values of 0.9978 and 0.9939, respectively, whereas the normalised flux model recorded values of 0.9911 and 0.9540.

Residual analysis was further used to evaluate the deviation between the experimental and predicted responses. The close agreement between predicted R^2 and adjusted R^2 values confirmed the adequacy and reliability of the developed model within the investigated operating range. The normal probability plots shown in Figures 5b and 6b demonstrated that the residuals were randomly distributed and followed an approximately linear trend, indicating normally distributed and statistically insignificant model errors. Externally studentised residuals were calculated by normalising the residual values using the estimated standard deviation to identify potential outlier observations. One outlier was detected at a pH of 3 and a concentration of 450 mg/L MO dye. This behaviour might be associated with the electrostatic repulsion of the CNF filter paper under low ZPC conditions. In this case, both the membrane surface and MO dye molecules were positively charged, and this decreased the interaction between them. The distribution of the residuals in Figure 5c and Figure 6c was random, which indicates that the regression model was appropriate to predict the behaviour of colour removal and normalised flux. Furthermore, the residual plots against the experimental runs in Figures 5d and 6d revealed that the standardised residual values were within the acceptable range of ±2, which showed that the quadratic response surface model is reasonably fitted.

Significant precision analysis was also carried out to assess the reliability of the developed regression model by considering the signal-to-noise ratio. Sidik et al. (2019) suggest that the values above 4 are considered acceptable model performances. The adequate precision value of colour removal was 64.6398, and the normalised flux was 44.7517 in this study. These values are indicative of a good response of the signal and foretell that the built model was appropriate for navigating the design space.

Table 6
Summary of RSM model fitting for the response variables

Response (Y_1): Colour Removal (%)							
Mean	**Std. dev.**	**R^2**	**Adj. R^2**	**Pred. R^2**	**C.V.**	**A.P.**	**PRESS**
71.76	0.9073	0.9991	0.9978	0.9939	1.26	64.64	26.91
Response (Y_2): Normalised Flux							
Mean	**Std. dev.**	**R^2**	**Adj. R^2**	**Pred. R^2**	**C.V.**	**A.P.**	**PRESS**
0.5497	0.0232	0.9963	0.9911	0.9540	4.23	44.75	0.0336

Note. Std. dev. = standard deviation; R^2 = coefficient of determination; Adj. R^2 = adjusted R^2; Pred. R^2 = predicted R^2; C.V. = coefficient of variance; A.P. = adequate precision and PRESS = predicted residual error sum of square

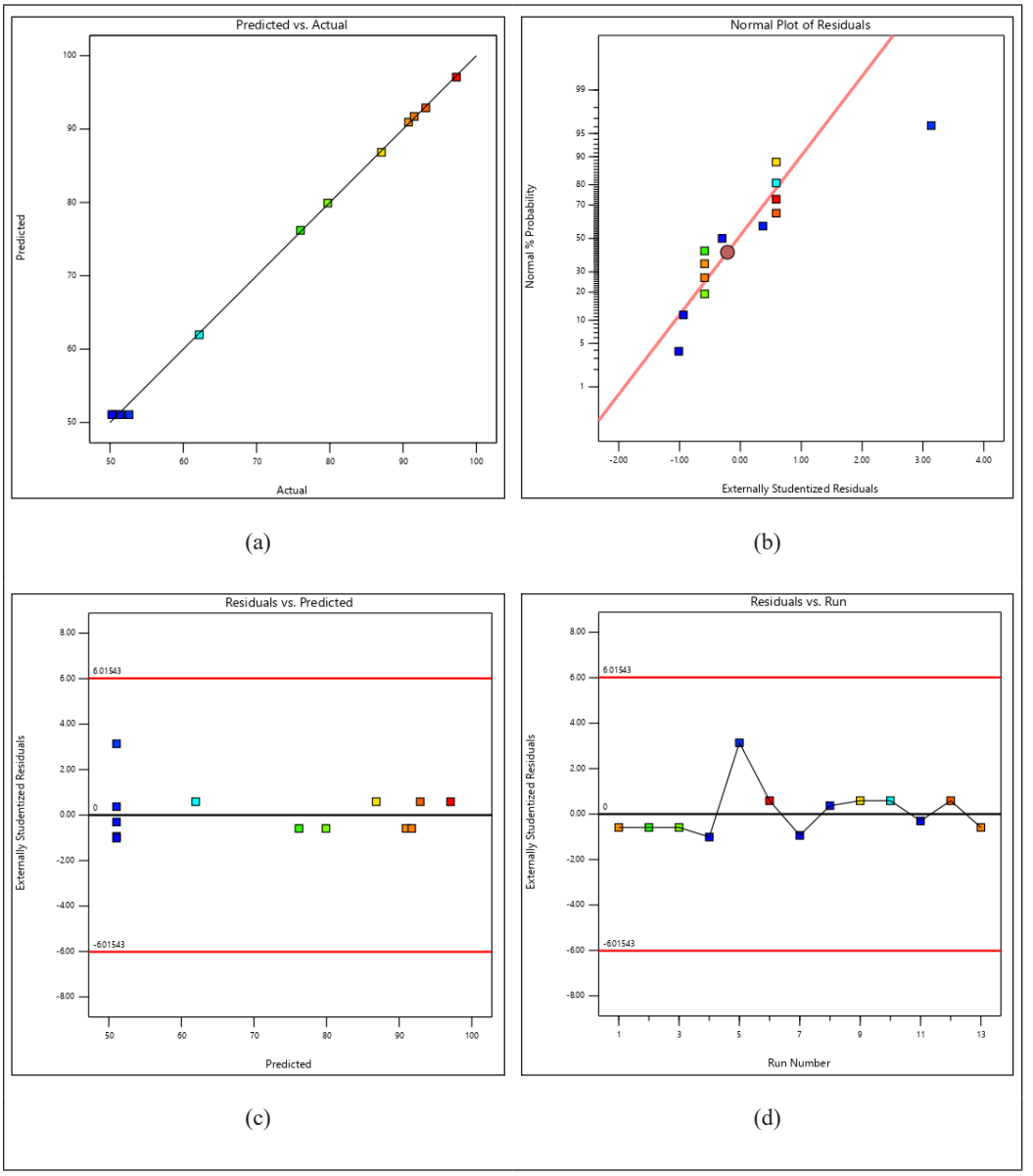

Figure 5. Residual diagnostic plots for the colour removal response consisting of (a) predicted versus actual response values; (b) normal probability plot of externally studentised residuals; (c) predicted residuals against externally studentised residuals; and (d) externally studentised residuals plotted against experimental runs

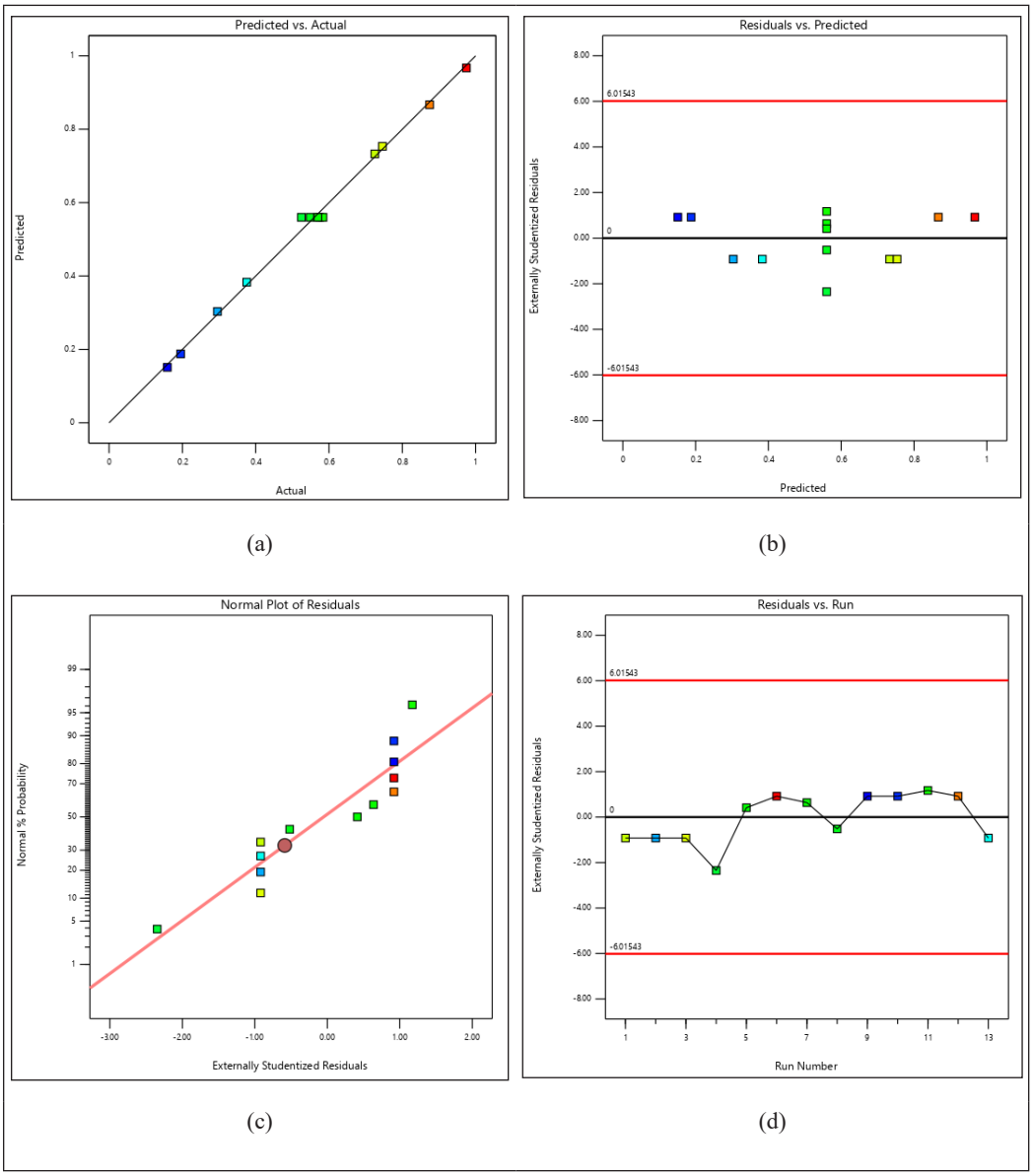

Figure 6. The normalised flux response is shown in the following plots using the residue analysis: (a) predicted vs experimental; (b) normal probability plot of externally studentised residuals; (c) predicted residuals vs externally studentised residuals; and (d) externally studentised residuals vs experimental runs

Influence of Independent Variables on Colour Removal and Normalised Flux Using CCD-RSM

The solution pH changed the surface charge properties of the CNF filter paper and the interaction between the MO dye molecules and the filter paper during filtration. The maximum colour removal efficiency (Y1) was found in an acidic medium. The pH removal efficiency gradually declined with increasing pH towards 6.5 and rose slightly at alkaline pH. The normalised flux (Y2), on the other hand, presented a negative trend as the pH increased. Accumulation of the MO dye on the surface of the filter paper during the filtration process had a close relationship with the filtration behaviour. The permeate flux was then more stable, which demonstrated the formation of a secondary fouling layer on the surface of the CNF filter paper (Satyanarayana et al., 2005).

The interaction between the solution pH and the isoelectric point (IEP) of the prepared filter paper was associated with the filtration performance. The IEP of the CNF filter paper was about 8.10, thus the surface was still positive at the pH levels below 8.1. This situation helped the electrostatic attraction of MO dye molecules (IEP ~3.47), which led to better removal of the dye under acidic conditions (Das et al., 2021). The interaction between the charged dye molecules and the filter paper surface was also shown in changes of flux behaviour. Chemical adsorption and interactions between the functional groups of the CNF structure could have played a role in the filtration behaviour, at higher pH conditions (Bandini & Mazzoni, 2005). Under strongly alkaline conditions (pH 9-10), however, the permeate flux is further reduced by electrostatic repulsion between the negatively charged dye molecules and the surface of the filter paper. This repulsion caused dye aggregation, and some of these dye aggregates were found to penetrate the void spaces and fibre network of the CNF filter paper.

The concentration of dye was also found to influence the filtration of the CNF filter paper. The increase in dye concentration was an indirect cause of flux reduction because it created a higher osmotic pressure inside the system (Hairom et al., 2014). For the colour removal response (Y1), two different trends were observed as the initial concentration of the MO dye was increased. As the concentration of the dye was raised, the removal efficiency decreased from about 83.10% to 72.60% before it gradually increased to 97.28% at 600 mg/L. The normalised flux, on the other hand, increased slightly in the intermediate concentration region. This behaviour may be linked to the interaction of the combined effect of osmotic pressure, dye adsorption, and electric double layer interaction on the filter paper's surface (Desa et al., 2019). Meanwhile, large dye accumulations on the filter paper surface resulted in more pronounced fouling behaviour in filtration.

Surface and Contour Plot Analysis

The response surfaces plotted in three dimensions (3D) show the interaction between the operating variables and the responses measured as peaks and curvature of the plots. Contour plots were drawn to show the influence of the combination of two independent variables - solution pH and initial dye concentration at three operating levels.

Figures 7a-d demonstrate the effect of initial MO dye concentration on solution pH for the CNF filter paper composition of 50:50. Response surfaces are shown that represent the filtration performance post 3 hours of operation in the crossflow filtration system for colour removal and normalised flux responses.

It can be observed in Figure 7a that under acidic conditions, the colour removal efficiency was higher at high dye concentration. The removal performance was also good with a combination of low dye concentration and alkaline pH, but moderate operating conditions yielded low removal efficiency. In the acidic pH range (4-6.5), the removal efficiency decreased from ~ 97.38% to 72.57% as the dye concentration varied from high to intermediate. The response surface at higher pH values (6.5-9) and dye concentrations (450-600mg/l) showed a more pronounced curvature, with colour removal gradually improving from 72.58% to 90.04%. The same pattern of behaviour is seen with the darker red area in the contour plot of Figure 7(b) representing higher response values. The optimum condition for MO dye removal based on the RSM optimisation analysis was achieved by using an initial dye concentration of 600mg/L at pH 4, which resulted in a 97.28% efficiency of colour removal.

It was found that higher colour removal in both acid and alkaline conditions might be associated with the aggregation of dye molecules during filtration. Possibly, the aggregated dye particles benefited with regard to their retention in the CNF filter paper in the interfibre bonding regions and void spaces. With the passage of time, during filtration, the deposited MO dye layers started to form on the surface of the filter paper and a secondary layer was formed, which contributed to a higher colour removal efficiency.

The response surface and contour plots of the normalised flux response are shown in Figures 7c and 7d, respectively. The normalised flux value increased (0.9748-0.9751) at higher dye concentration (540 to 600 mg/L) under acidic condition as shown by the darker region in the contour plot. Lower responses to the flux, however, were primarily seen around pH 6.5 and dye concentrations of 300 to 450 mg/L with normalised flux ranging from 0.2738 to 0.2869. Additional flux reductions were observed at pH 9 under 600mg/l dye concentration and at pH 4 under 300mg/l dye concentration with normalised flux value of 0.0589 and 0.0745 respectively.

The observed behaviour can be associated with the formation of a compact dye deposition layer on the CNF filter paper surface. This accumulated layer functioned as a secondary filtration barrier, limiting the transport of treated dye solution through

the filter and subsequently reducing the normalised flux. The flux response in this study displayed an unstable trend similar to the colour removal behaviour, particularly as the pH and initial dye concentration increased. Similar findings were reported by Ricceri et al. (2022), who investigated fouling behaviour in membrane distillation systems optimised using CCD with inlet temperature and crossflow velocity as operating variables. Their study showed that fouling formation did not exhibit a consistent relationship with the investigated variables, resulting in unstable flux decline behaviour caused by variations in fouling layer thickness on the membrane surface.

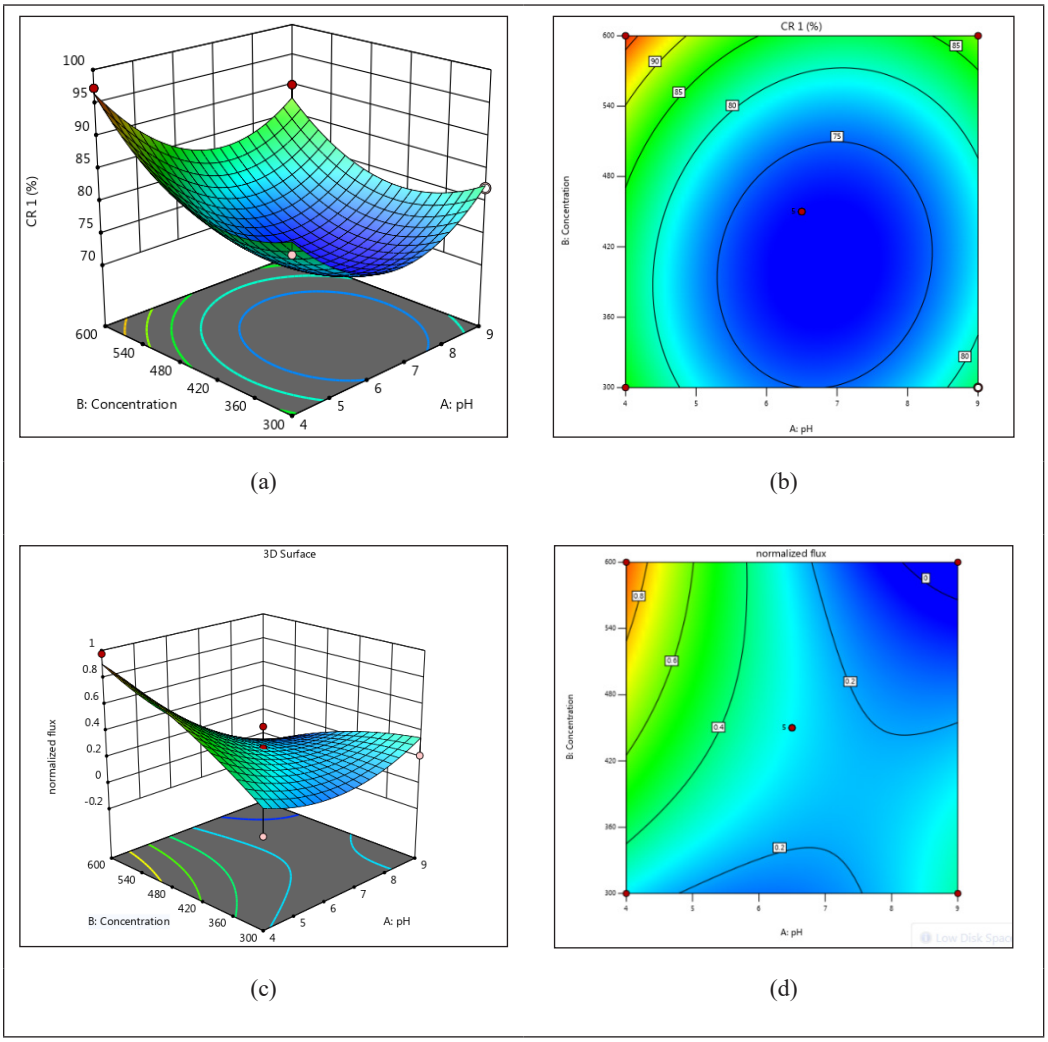

Figure 7. 3D response surface and contour plots showing the combined effects of initial MO dye concentration and solution pH on (a, b) colour removal efficiency and (c, d) normalised flux for the 50:50 CNF filter paper composition

Model Optimisation and Validation

The objective of the optimisation procedure was to identify the optimum operating conditions from the experimental design for achieving the targeted filtration responses (Veza et al., 2023). A desirability function method was employed to simultaneously maximise colour removal percentage and normalised flux. The desirability function ranges from 0 to 1, where 0 indicates responses outside the acceptable range and 1 represents complete fulfilment of the optimisation objective (Ebba et al., 2022; Saeed et al., 2015). The CCD-RSM model predicted optimum conditions at pH 4 and 600 mg/L initial MO dye concentration using a 50:50 cellulose dosage ratio. At these conditions, the predicted responses were 97.28% colour removal and 0.9748 normalised flux. Experimental validation was subsequently performed in triplicate to confirm the reliability of the optimised model predictions.

The fabricated *Neolamarckia cadamba* CNF filter paper was compared with different nanocellulose based materials reported in literature. The developed filter paper demonstrated a similar effectiveness to filters based on wood cellulose, as reported by Mautner and Bismarck (2021) in regard to the ability to reject dyes. But the current system showed higher flux holding potential during filtration. It was previously reported that wood pulp derived membranes and bacterial cellulose networks were able to reach high rejection percentages around 95%~98%, however, they were generally operated under the dead-end filtration mode, and the permeabilities of the membranes were very low. Similarly, bamboo-derived cellulose materials and adsorbents with agricultural waste also showed good dye removal efficiencies from 88% to 92.4%. However, many of these systems were constrained by low density or batch adsorption process rather than a continuous filtration process (Wu et al., 2017).

The optimum operating conditions and corresponding predicted responses for colour removal and normalised flux for MO dye treatment are summarised in Table 7. Experimental data showed good agreement with the model-predicted values, which suggested the developed CCD-RSM model was adequate to describe the performance of the CNF filter paper for the crossflow filtration system. Moosazade et al. (2021) studied the removal of Pb from water using CCD-RSM optimisation in an electrocoagulation-flotation system and obtained a maximum removal efficiency of ~97.28% at an electrolysis time of 77.65 min and a current of 0.9 A. The optimisation method used in this study also demonstrated good ability to optimise the operating conditions of textile wastewater treatment with minimum difference between the predicted and experimental responses as reported by Hermosilla et al. (2009).

Table 7
Optimum conditions and laboratory experiment validation

Response (Y_1): Colour Removal (%)					
Run	**pH**	**Initial MO dye Concentration (mg/L)**	**Experimental Condition**	**Predicted Condition**	**Error (%)**
1	4	600	97.28	96.79	-0.51
2	4	600	96.31	96.79	0.50
3	4	600	96.78	96.79	0.01
Response (Y_2): Normalised Flux					
Run	**pH**	**Initial MO dye Concentration (mg/L)**	**Experimental Condition**	**Predicted Condition**	**Error (%)**
1	4	600	0.9748	0.9801	0.54
2	4	600	0.9874	0.9801	-0.74
3	4	600	0.9781	0.9801	0.20

To test the predictive ability of the developed model, six validation experiments were carried out with operating conditions not covered in the original CCD data. It has been reported that a few experimental points may be enough to validate and do not necessarily represent the predictive ability of the developed model (Hamid et al., 2016). So, six operating conditions with different unseen factors were chosen to obtain a more comprehensive evaluation of the model applicability, as shown in Table 8. These validation runs were done inside and outside the range of the original experiments. Good agreement was seen between the predicted and experimental results for the residual values obtained for both responses studied. In general, the RSM models could predict the responses in the original CCD experiments and the additional validation experiments with acceptable accuracy.

Table 8
Validation of the developed model using unseen experimental conditions

Response (Y_1): Colour Removal (%)						
Run	**pH**	**Initial MO dye Concentration (mg/L)**	**Cellulose Dosage**	**Experimental**	**Predicted**	**Residual Error %**
1	3	100	60:40	85.34	87.04	-1.99
2	7	100	70:30	86.78	88.76	-2.28
3	10	100	80:20	90.10	89.98	0.13
4	3	300	60:40	62.11	63.05	-1.51
5	7	300	70:30	71.00	69.78	1.72
6	10	300	80:20	75.49	77.32	-2.42

Table 8 (*continued*)

Response (Y_2): Normalised Flux						
Run	**pH**	**Initial MO dye Concentration (mg/L)**	**Cellulose Dosage**	**Experimental**	**Predicted**	**Residual Error %**
1	3	100	60:40	0.1400	0.1387	0.93
2	7	100	70:30	0.9664	0.9867	-2.10
3	10	100	80:20	0.3211	0.3512	-9.37
4	3	300	60:40	0.2687	0.2500	6.96
5	7	300	70:30	0.9037	0.9157	-1.33
6	10	300	80:20	0.1251	0.131	-6.39

Membrane Fouling Mechanism Analysis

The membrane fouling behaviour under the optimum synthetic dye treatment conditions using the CNF filter paper in the crossflow filtration system was analysed in this study. The fitting profile of the obtained data by the Wiesner and Aptel equations is presented in Figure 8, and the respective R^2 values and fitted rate constants (K) are summarised in Table 9 for fouling model evaluation.

Analysis revealed that cake layer formation was the major fouling mechanism in the first and second stages of filtration, with R2 values of 0.9528 and 0.9456, respectively. The observed gel/cake layer developed from the accumulation and coagulation of pollutant molecules retained on the CNF filter paper surface. Progressive deposition of these foulants reduced the permeate flux throughout the filtration process while improving the overall colour removal efficiency. This behaviour is consistent with the optimum filtration performance obtained in this study, which achieved 97.28% colour removal and a normalised flux of 0.9748. The sharp decrease in permeate flux observed at the early stage of filtration further suggested rapid development of the cake layer as the primary fouling mechanism. Similar observations have been reported in previous nanofiltration studies, where cake formation was identified as the primary contributor to flux decline behaviour (Sidik et al., 2019). The fouling behaviour may be associated with the larger size of MO dye particles relative to the void spaces within the CNF fibre network, promoting dye deposition and dense cake layer formation on the filter paper surface (Cerón-Vivas et al., 2019; Zhang et al., 2021). However, the complete blocking, intermediate blocking, and standard blocking models showed weak agreement with the experimental data for both filtration stages, with R^2 values lower than 0.9. These findings suggest that the membrane fouling behaviour under optimum conditions followed a two-step cake layer formation mechanism.

Table 9
Rate constant and correlation of determination (R^2) values for CNF filter paper fouling mechanisms at optimum conditions

Blocking Filtration Laws	CNF Filter Paper (50:50)			
	Stage 1		Stage 2	
	R^2	K (s^{-1})	R^2	K (s^{-1})
Complete Blocking	< 0.1	< 0.1	< 0.1	< 0.1
Intermediate Blocking	0.7391	7.257	0.3539	3.544
Standard Blocking	0.3864	2.475	< 0.1	0.9054
Cake Formation	0.9528	34.80	0.9456	34.03

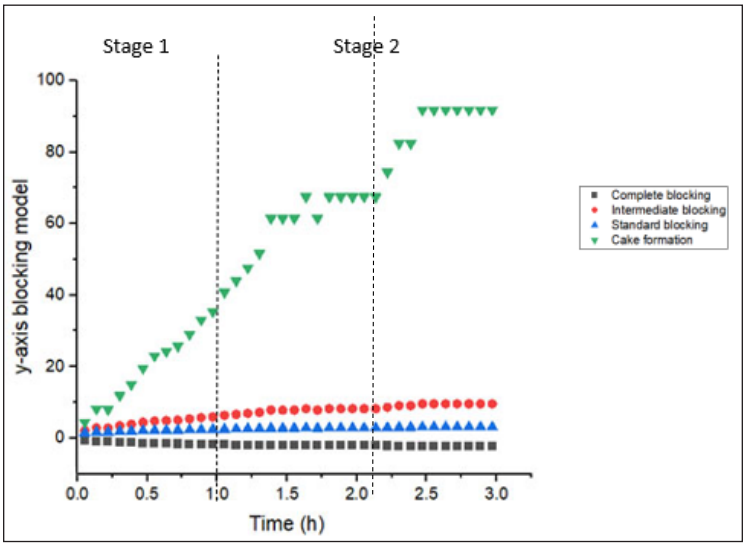

Figure 8. Fouling mechanism analysis of CNF filter paper under optimum filtration conditions (50:50 cellulose dosage ratio, pH 4, and 600 mg/L initial MO dye concentration)

CHALLENGES AND FUTURE PERSPECTIVES OF CNF FILTER PAPER

The practical application of *Neolamarckia cadamba* CNF filter paper in industrial textile wastewater treatment is supported by its economic and operational feasibility. From an economic perspective, *Neolamarckia cadamba* (locally known as Kelempayan) is a fast-growing Malaysian plantation species that provides a sustainable and low-cost feedstock compared to synthetic polymers. However, there were limitations in terms of the durability and resilience of the fabricated nanopapers during extended contact times. There is a need for further advances in the production of CNF filter papers with enhanced mechanical stability and durability of the nanocellulose fibre network. It is still essential to maintain an appropriate density and porosity for adequate filtration.

The fabricated filter paper may also have better reusability potential due to better structural stability.

CONCLUSION

This work aimed to study the optimisation of MO dye removal by the CNF filter paper in the crossflow filtration system. CCD and RSM were used to identify the conditions that resulted in high colour removal and acceptable normalised flux performance. The results indicated that the pH of the solution, and the initial dye concentration of MO significantly influenced the filtration behaviour of the prepared CNF filter paper. The optimum operating condition was determined as a 50:50 cellulose dosage ratio, an initial MO dye concentration of 600 mg/L and a pH of 4 from the optimisation analysis under high desirability conditions. These developed quadratic models exhibited good correlations with the experimental data, with R^2 of 0.9991 for colour removal and R^2 of 0.9963 for normalised flux. The maximum colour removal (97.28%) and normalised flux (0.9748) of the crossflow filtration system were obtained under optimum conditions. Fouling analysis showed that fouling during filtration was primarily attributed to the formation of a cake layer, which primarily occurred due to the interaction of the MO dye solution with the surface of the CNF filter paper. The results of the overall fabricated *Neolamarckia cadamba* CNF filter paper indicated that it is a potential sustainable filtration material for industrial wastewater treatment applications with good filtration behaviour and high removal performance.

ACKNOWLEDGEMENT

This research was supported by Universiti Tun Hussein Onn Malaysia (UTHM) through Tier 1 (Vot Q991) and Postgraduate Research Grant (GPPS, Vot Q787). The authors would like to acknowledge Forest Research Institute Malaysia (FRIM) for providing the laboratory instrument for this study.

REFERENCES

Amin, I. N. H. M., & Nizam, M. H. M. (2016). Assessment of membrane fouling indices during removal of reactive dye from batik wastewater. *Journal of Water Reuse and Desalination*, *6*(4), 505-514. https://doi.org/10.2166/wrd.2016.072

Aryanti, N., Saraswati, A., Pratama Putra, R., Nafiunisa, A., & Hesti Wardhani, D. (2018). Fouling mechanism of micelle enhanced ultrafiltration with SDS surfactant for indigozol dye removal. *Jurnal Teknologi, 80*(3), 101-108. https://doi.org/10.11113/jt.v80.12741

Bai, Y., Wu, Y. H., Wang, R. N., Xue, S., Chen, Z., & Hu, H. Y. (2023). Critical minority fractions causing membrane fouling in reclaimed water: Fouling characteristics, mechanisms and control strategies. *Environment International*, *173*, Article 107818. https://doi.org/10.1016/j.envint.2023.107818

Cerón-Vivas, A., Cáceres, K. T., Rincón, A., & Cajigas, A. (2019). Influence of pH and the C/N ratio on the biogas production of wastewater. *Revista Facultad de Ingeniería*, *92*, 88-95. https://doi.org/10.17533/udea.redin.20190627

Das, L., Das, P., Bhowal, A., & Bhattacharjee, C. (2021). Enhanced biosorption of fluoride by extracted nanocellulose/polyvinyl alcohol composite in batch and fixed-bed system: ANN analysis and numerical modelling. *Environmental Science and Pollution Research*, *28*(34), 47107-47125. https://doi.org/10.1007/s11356-021-14026-x

Desa, A. L., Hairom, N. H. H., Ng, L. Y., Ng, C. Y., Ahmad, M. K., & Mohammad, A. W. (2019). Industrial textile wastewater treatment via membrane photocatalytic reactor (MPR) in the presence of ZnO-PEG nanoparticles and tight ultrafiltration. *Journal of Water Process Engineering*, *31*, Article 100872. https://doi.org/10.1016/j.jwpe.2019.100872

Ebba, M., Asaithambi, P., & Alemayehu, E. (2022). Development of electrocoagulation process for wastewater treatment: optimisation by response surface methodology. *Heliyon*, *8*(5), Article e09383. https://doi.org/10.1016/j.heliyon.2022.e09383

El-Sheekh, M. M., El-Nagar, A. A., ElKelawy, M., & Bastawissi, H. A. E. (2023). Maximisation of bioethanol productivity from wheat straw, performance and emission analysis of diesel engine running with a triple fuel blend through response surface methodology. *Renewable Energy*, *211*, 706-722. https://doi.org/10.1016/j.renene.2023.04.145

Esmi, F., Dalai, A. K., & Hu, Y. (2023). Optimisation and kinetic studies of 12-tungstophosphoric supported mesoporous aluminosilicate through response surface methodology for biodiesel production using green seed canola oil. *Fuel*, *348*, Article 128594. https://doi.org/10.1016/j.fuel.2023.128594

Favier, L., Andrei-Ionuț Simion, Hlihor, R. M., Fekete-Kertész, I., Molnár, M., Harja, M., & Vial, C. (2023). Intensification of the photodegradation efficiency of an emergent water pollutant through process conditions optimisation by means of response surface methodology. *Journal of Environmental Management*, *328*, Article 116928. https://doi.org/10.1016/j.jenvman.2022.116928

Hairom, N. H. H., Mohammad, A. W., & Kadhum, A. A. H. (2014). Nanofiltration of hazardous Congo red dye: Performance and flux decline analysis. *Journal of Water Process Engineering*, *4*, 99-106. https://doi.org/10.1016/j.jwpe.2014.09.008

Hairom, N. H. H., Mohammad, A. W., & Kadhum, A. A. H. (2015). Influence of zinc oxide nanoparticles in the nanofiltration of hazardous Congo red dyes. *Chemical Engineering Journal*, *260*, 907-915. https://doi.org/10.1016/j.cej.2014.08.068

Hamid, H. A., Jenidi, Y., Thielemans, W., Somerfield, C., & Gomes, R. L. (2016). Predicting the capability of carboxylated cellulose nanowhiskers for the remediation of copper from water using response surface methodology (RSM) and artificial neural network (ANN) models. *Industrial Crops and Products*, *93*, 108-120. https://doi.org/10.1016/j.indcrop.2016.05.035

Hanafy, H. (2021). Adsorption of methylene blue and bright blue dyes on bayleaf capertree pods powder: Understanding the adsorption mechanism by a theoretical study. *Journal of Molecular Liquids*, *332*, Article 115680. https://doi.org/10.1016/j.molliq.2021.115680

Hermia, J. (1985). Blocking Filtration. Application to non-Newtonian fluids. In A. Rushton (Ed.), *Mathematical models and design methods in solid-liquid separation* (pp. 83-89). Springer Netherlands. https://doi.org/10.1007/978-94-009-5091-7_5

Hermosilla, D., Cortijo, M., & Huang, C. P. (2009). Optimising the treatment of landfill leachate by conventional Fenton and photo-Fenton processes. *Science of the Total Environment*, *407*(11), 3473-3481. https://doi.org/10.1016/j.scitotenv.2009.02.009

Hussain, S., Kamran, M., Khan, S. A., Shaheen, K., Shah, Z., Suo, H., Khan, Q., Shah, A. B., Rehman, W. U., Al-Ghamdi, Y. O., & Ghani, U. (2021). Adsorption, kinetics and thermodynamics studies of methyl orange dye sequestration through chitosan composites films. *International Journal of Biological Macromolecules*, *168*, 383-394. https://doi.org/10.1016/j.ijbiomac.2020.12.054

Janesch, J., Jones, M., Bacher, M., Kontturi, E., Bismarck, A., & Mautner, A. (2020). Mushroom-derived chitosan-glucan nanopaper filters for the treatment of water. *Reactive and Functional Polymers*, *146*, Article 104428. https://doi.org/10.1016/j.reactfunctpolym.2019.104428

Javaid, R., Qazi, U. Y., Ikhlaq, A., Zahid, M., & Alazmi, A. (2021). Subcritical and supercritical water oxidation for dye decomposition. *Journal of Environmental Management*, *290*, Article 112605. https://doi.org/10.1016/j.jenvman.2021.112605

Jiang, Z., & Hu, D. (2019). Molecular mechanism of anionic dyes adsorption on cationized rice husk cellulose from agricultural wastes. *Journal of Molecular Liquids*, *276*, 105-114. https://doi.org/10.1016/j.molliq.2018.11.153

K, A., Mungray, A., Agarwal, S., Ali, J., & Chandra Garg, M. (2021). Performance optimisation of forward-osmosis membrane system using machine learning for the treatment of textile industry wastewater. *Journal of Cleaner Production*, *289*, Article 125690. https://doi.org/10.1016/j.jclepro.2020.125690

Kadier, A., Wang, J., Chandrasekhar, K., Abdeshahian, P., Islam, M. A., Ghanbari, F., Bajpai, M., Katoch, S. S., Bhagawati, P. B., Li, H., Kalil, M. S., Hamid, A. A., Abu Hasan, H., & Ma, P. C. (2022). Performance optimisation of microbial electrolysis cell (MEC) for palm oil mill effluent (POME) wastewater treatment and sustainable Bio-H2 production using response surface methodology (RSM). *International Journal of Hydrogen Energy*, *47*(34), 15464-15479. https://doi.org/10.1016/j.ijhydene.2021.09.259

Latifah, J., Nurrul-Atika, M., Sharmiza, A., & Rushdan, I. (2020). Extraction of nanofibrillated cellulose from kelempayan (*Neolamarckia cadamba*) and its use as strength additive in papermaking. *Journal of Tropical Forest Science*, *32*(2), https://doi.org/10.26525/jtfs32.2.170

Mautner, A., & Bismarck, A. (2021). Bacterial nanocellulose papers with high porosity for optimised permeance and rejection of nm-sized pollutants. *Carbohydrate Polymers*, *251*, Article 117130. https://doi.org/10.1016/j.carbpol.2020.117130

Mautner, A., Kwaw, Y., Weiland, K., Mvubu, M., Botha, A., John, M. J., Mtibe, A., Siqueira, G., & Bismarck, A. (2019). Natural fibre-nanocellulose composite filters for the removal of heavy metal ions from water. *Industrial Crops and Products*, *133*(March), 325-332. https://doi.org/10.1016/j.indcrop.2019.03.032

Miao, R., Ma, B., Li, P., Wang, P., Wang, L., & Li, X. yan. (2021). Mitigation mechanism of ozonation in the casein fouling of ultrafiltration membranes: Possible application in dairy wastewater treatment. *Journal of Membrane Science*, *629*, Article 119307. https://doi.org/10.1016/j.memsci.2021.119307

Moosazade, M., Ashoori, R., Moghimi, H., Amani, M. A., Frontistis, Z., & Taheri, R. A. (2021). Electrochemical recovery to overcome direct osmosis concentrate-bearing lead: Optimisation of treatment process via RSM-CCD. *Water*, *13*(21), Article 3136. https://doi.org/10.3390/w13213136

Norrahma, S. S. A., Hamid, N. H. A., Hairom, N. H. H., Jasmani, L., & Sidik, D. A. B. (2023). Industrial textile wastewater treatment using *Neolamarckia cadamba* NFC filter paper via cross-flow filtration system. *Journal of Water Process Engineering*, *55*, Article 104188. https://doi.org/10.1016/j.jwpe.2023.104188

Petcu, A. R., Lazar, C. A., Rogozea, E. A., Olteanu, N. L., Meghea, A., & Mihaly, M. (2016). Nonionic microemulsion systems applied for removal of ionic dyes mixtures from textile industry wastewaters. *Separation and Purification Technology*, *158*, 155-159. https://doi.org/10.1016/j.seppur.2015.12.002

Pu, Y., Tang, J., Zeng, T., Hu, Y., Wang, Q., Huang, J., Pan, S., Wang, X. C., Li, Y., Hao Ngo, H., & Abomohra, A. (2022). Enhanced energy production and biological treatment of swine wastewater using anaerobic membrane bioreactor: Fouling mechanism and microbial community. *Bioresource Technology*, *362*, Article 127850. https://doi.org/10.1016/j.biortech.2022.127850

Ricceri, F., Blankert, B., Ghaffour, N., Vrouwenvelder, J. S., Tiraferri, A., & Fortunato, L. (2022). Unravelling the role of feed temperature and cross-flow velocity on organic fouling in membrane distillation using response surface methodology. *Desalination*, *540*, Article 115971. https://doi.org/10.1016/j.desal.2022.115971

Saeed, M. O., Azizli, K., Isa, M. H., & Bashir, M. J. K. (2015). Application of CCD in RSM to obtain optimised treatment of POME using Fenton oxidation process. *Journal of Water Process Engineering*, *8*, e7-e16. https://doi.org/10.1016/j.jwpe.2014.11.001

Satyanarayana, T., Raghukumar, C., & Shivaji, S. (2005). Extremophilic microbes: Diversity and perspectives. *Current Science*, *89*(1), 78-90.

Septevani, A. A., Rifathin, A., Sari, A. A., Sampora, Y., Ariani, G. N., Sudiyarmanto, & Sondari, D. (2020). Oil palm empty fruit bunch-based nanocellulose as a super-adsorbent for water remediation. *Carbohydrate Polymers*, *229*, Article 115433. https://doi.org/10.1016/j.carbpol.2019.115433

Sidik, D. A. B., Hairom, N. H. H., & Mohammad, A. W. (2019). Performance and fouling assessment of different membrane types in a hybrid photocatalytic membrane reactor (PMR) for palm oil mill secondary effluent (POMSE) treatment. *Process Safety and Environmental Protection*, *130*, 265-274. https://doi.org/10.1016/j.psep.2019.08.018

Singh, M., Vajpayee, M., & Ledwani, L. (2021). Eco-friendly surface modification of natural fibres to improve dye uptake using natural dyes and application of natural dyes in fabric finishing: A review. *Materials Today: Proceedings*, *43*, 2868-2871. https://doi.org/10.1016/j.matpr.2021.01.078

Thiruppathi, K., Rangasamy, K., Ramasamy, M., & Muthu, D. (2021). Evaluation of textile dye degrading potential of ligninolytic bacterial consortia. *Environmental Challenges*, *4*, Article 100078. https://doi.org/10.1016/j.envc.2021.100078

Türgay, O., Ersöz, G., Atalay, S., Forss, J., & Welander, U. (2011). The treatment of azo dyes found in textile industry wastewater by anaerobic biological method and chemical oxidation. *Separation and Purification Technology*, *79*(1), 26-33. https://doi.org/10.1016/j.seppur.2011.03.007

Veza, I., Spraggon, M., Fattah, I. M. R., & Idris, M. (2023). Response surface methodology (RSM) for optimising engine performance and emissions fueled with biofuel: Review of RSM for sustainability energy transition. *Results in Engineering*, *18*, Article 101213. https://doi.org/10.1016/j.rineng.2023.101213

Wiesner, & Aptel. (1996). Mass transport and permeate flux and fouling in pressure-driven processes. In M. R. Wiesner & P. Aptel (Eds.), *Water treatment membrane conditions handbook.* McGraw-Hill.

Wu, B., Geng, B., Chen, Y., Liu, H., Li, G., & Wu, Q. (2017). *Preparation and characteristics of TEMPO-oxidised cellulose nanofibrils from bamboo pulp and their oxygen-barrier application in PLA films*. Frontiers of Chemical Science and Engineering. 11. 1-10. https://doi.org/10.1007/s11705-017-1673-8

Yadav, S., Yadav, A., Bagotia, N., Sharma, A. K., & Kumar, S. (2021). Adsorptive potential of modified plant-based adsorbents for sequestration of dyes and heavy metals from wastewater - A review. *Journal of Water Process Engineering*, *42*, Article 102148. https://doi.org/10.1016/j.jwpe.2021.102148

Yousefi, N., Jones, M., Bismarck, A., & Mautner, A. (2021). Fungal chitin-glucan nanopapers with heavy metal adsorption properties for ultrafiltration of organic solvents and water. *Carbohydrate Polymers*, *253*, Article 117273. https://doi.org/10.1016/j.carbpol.2020.117273

Zhang, W., Zhang, Y., Cao, J., & Jiang, W. (2021). Improving the performance of edible food packaging films by using nanocellulose as an additive. *International Journal of Biological Macromolecules*, *166*, 288-296. https://doi.org/10.1016/j.ijbiomac.2020.10.185

Zhou, H., Zhang, M., Chen, Q., Shan, Q., Liu, S., Lin, J., Ma, L., Zheng, G., Li, L., Zhao, C., Wei, L., Dai, X., & Yin, Y. (2023). Determination of amphenicol antibiotic residues in aquaculture products by response surface methodology modified QuEChERS method combined with UPLC-MS/MS. *Microchemical Journal*, *190*, Article 108729. https://doi.org/10.1016/j.microc.2023.108729